NASA TECHNICAL MEMORANDUM

NASA TM X-62,490

NASA TM X-62,490

A DESIGN METHOD FOR ENTRANCE SECTIONS OF TRANSONIC WIND TUNNELS WITH RECTANGULAR CROSS SECTIONS

Lionel L. Levy, Jr. and John B. McDevitt

Ames Research Center
Moffett Field, Calif. 94035

September 1975

1. Report No.	2. Government Accession No.	3. Recipient's Catalog No.
TM X-62,490		

4. Title and Subtitle	5. Report Date
A DESIGN METHOD FOR ENTRANCE SECTIONS OF TRANSONIC WIND TUNNELS WITH RECTANGULAR CROSS SECTIONS	6. Performing Organization Code A-6293

7. Author(s)	8. Performing Organization Report No.
Lionel L. Levy, Jr. and John B. McDevitt	

9. Performing Organization Name and Address	10. Work Unit No. 505-06-13
NASA Ames Research Center Moffett Field, Calif. 94035	11. Contract or Grant No.

12. Sponsoring Agency Name and Address	13. Type of Report and Period Covered Technical Memorandum
National Aeronautics and Space Administration Washington, D. C. 20546	14. Sponsoring Agency Code

15. Supplementary Notes

16. Abstract

A technique has been developed to design entrance sections for transonic or high-speed subsonic wind tunnels with rectangular cross sections which satisfies two important requirements: (1) the transition from a circular cross-section settling chamber to a rectangular test section is accomplished smoothly so as not to introduce secondary flows (vortices or boundary-layer separation) into a uniform test stream and (2) the transition is accomplished within a specified length. The mathematical technique for shaping the entrance section is described and the results of static-pressure measurements in the transition region and of static- and total-pressure surveys in the test section of a pilot model for a new facility at the Ames Research Center are presented..

17. Key Words (Suggested by Author(s))	18. Distribution Statement
Transonic flow Circular stagnation chamber Rectangular test section	Unlimited STAR Category– 02

19. Security Classif. (of this report)	20. Security Classif. (of this page)	21. No. of Pages	22. Price*
Unclassified	Unclassified	35	$3.75

*For sale by the National Technical Information Service, Springfield, Virginia 22151

A DESIGN METHOD FOR ENTRANCE SECTIONS OF TRANSONIC WIND TUNNELS WITH RECTANGULAR CROSS SECTIONS

By Lionel L. Levy, Jr. and John B. McDevitt

Ames Research Center
Moffett Field, Calif. 94035

ABSTRACT

A technique has been developed to design entrance sections for transonic or high-speed subsonic wind tunnels with rectangular cross sections which satisfies two important requirements: (1) the transition from a circular cross-section settling chamber to a rectangular test section is accomplished smoothly so as not to introduce secondary flows (vortices or boundary-layer separation) into a uniform test stream and (2) the transition is accomplished within a specified length. The mathematical technique for shaping the entrance section is described and the results of static-pressure measurements in the transition region and of static- and total-pressure surveys in the test section of a pilot model for a new facility at the Ames Research Center are presented.

INTRODUCTION

A High Reynolds Number Channel is currently operating at the Ames Research Center. It is being used to conduct experimental studies, over a wide range of Reynolds numbers, that are specifically designed to provide information relevant to the development and evaluation of advanced computer codes for numerically simulating transonic flows. A schematic of the facility is shown in figure 1. The tunnel, with various test channels of approximately 0.1 square meter (one square-foot) cross-sectional area, will provide transonic air flows with Reynolds numbers per meter ranging from 3×10^6 to 120×10^6

A schematic of the settling chamber, entrance section, and the first test channel to be employed (designed for tests of airfoil sections at high subsonic Mach numbers) is shown in figure 2. A technique used to design the entrance section that involves a transition from the circular cross section of the settling chamber to the rectangular cross section of the test section is described in this paper. Also included are the results of static- and total-pressure surveys made in a pilot model (40 percent scale) of the entrance and test sections for the new facility

ENTRANCE-SECTION DESIGN METHOD

The problem of designing a general three-dimensional wind-tunnel entrance section of finite length has not been solved analytically. In reference 1, Tsien obtained a series solution to the axisymmetric incompressible irrotational flow equations for an infinite conical-shaped entrance

section. The coefficients of the series were evaluated using derivatives of a specified velocity distribution along the axis. In reference 2 Thwaites obtained a series solution to the same equations for potential flow between two equipotential planes normal to the axis. The length and entrance- and exit-radii of the entrance section can be specified and the coefficients of the series evaluated by satisfying either of two conditions. One choice insures as uniform a velocity as possible across the entrance of the section; the other insures a monotonically increasing velocity distribution along the walls. While both of these characteristics of the flow are highly desirable, they cannot be achieved simultaneously using either choice for evaluating the series coefficients, at least not for a practical, finite number of terms.

The present design method combines certain features from references 1 and 2. The infinite-length solution of Tsien is examined to establish a set of "control points" (dimensions) to insure a monotonically increasing velocity in the high-velocity portion of the entrance section. Thwaites' finite-length solution is then found so that it passes through these control points and insures as uniform a velocity as possible across the entrance section. The resulting solution is tailored to a specified entrance-section length to obtain the axial area distribution. A smooth transition from a circular to a rectangular cross section is effected by maintaining the predetermined area distribution and satisfying specified slopes.

Control Points from Tsien's Axisymmetric Solution

Tsien's solution, which is used in the present case as a guide for specifying the contraction ratio and length of the high-speed portion of the entrance cone, is graphically summarized in figure 3. The streamlines for which the velocity exceeds the final exit value are shown as dashed lines (streamlines "E" and "F"). Thus, the contraction cone should be designed for a wall shape inside of streamline E in order to insure that the velocity does not overshoot near the wall. For all the streamlines, r(x), shown in figure 3(b), $r(0)/r(2) \approx 1.34$, which corresponds to a contraction ratio of $A(0)/A(2) \approx 1.8$. For the present design, a contraction ratio of 2, and axial length of 3 r(2) (corresponding to a streamline between B & C of fig. 3) were chosen for the high-speed portion of the entrance section. This conservative approach (a wall streamline well within E) was prompted by a consideration of compressibility effects (ref. 3).

The foregoing choice of area ratio and axial distance establishes two control points for the high-velocity end of the entrance section, points A and B in figure 4. A streamline that has a monotonically increasing velocity is desired which passes through these points and joins smoothly with the settling-chamber wall within some practical maximum length, L_{max}, predetermined by available space. Several satisfactory solutions may be possible as indicated by the dashed lines in figure 4. This problem is similar to that solved by Thwaites (ref. 2) in which the entrance-section length and contraction ratio are given and a shape determined. A brief description of Thwaites' method and its application to the present problem are presented next.

Thwaites' Axisymmetric Solution Fit to Control Points

The velocity potential that Thwaites gives is rewritten in a scaled form that is useful in designing a wind-tunnel entrance section with a specified length and end radii. Thus, with reference to sketch (a),

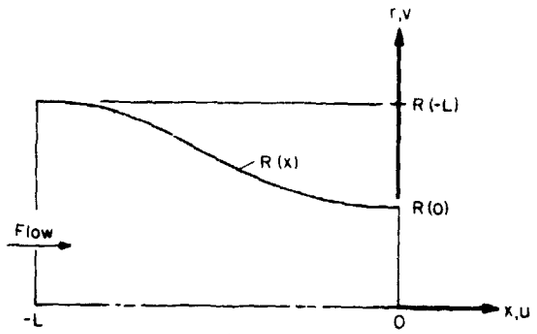

Sketch (a)

$$\phi(x,r) = \frac{L}{\pi}\left\{ a_0\left(\frac{\pi x}{L}\right) + \sum_{k=1}^{N} \frac{a_k}{k} \sin\left(k\frac{\pi x}{L}\right) I_0\left(k\frac{\pi r}{L}\right)\right\} \tag{1}$$

where L is the entrance-section length, I_0 is the modified Bessel's function of the second kind and order zero, and x and r are coordinates in the axial and radial directions. The velocity components, u, v, in these respective directions are given by

$$u = \frac{\partial \phi}{\partial x} = a_0 + \sum_{k=1}^{N} a_k \cos\left(k\frac{\pi x}{L}\right) I_0\left(k\frac{\pi r}{L}\right) \tag{2}$$

$$v = \frac{\partial \phi}{\partial r} = \sum_{k=1}^{N} a_k \sin\left(k\frac{\pi x}{L}\right) I_1\left(k\frac{\pi r}{L}\right) \tag{3}$$

and the scaled stream function is given by

$$\psi(x,r) = \left(\frac{\pi}{L}\right)^2 \int_0^r ur\, dr = \frac{1}{2} a_0 \left(\frac{\pi r}{L}\right)^2 + \left(\frac{\pi r}{L}\right) \sum_{k=1}^{N} \frac{a_k}{k} \cos\left(k\frac{\pi x}{L}\right) I_1\left(k\frac{\pi r}{L}\right) \tag{4}$$

The bounding streamline through R(0) and R(−L) in sketch (a) and the nature of the internal flow depend upon the manner in which the a_k coefficients of the series are evaluated. Two choices are available. One insures as uniform a velocity as possible across the entrance of the section, the other insures a monotonically increasing velocity along the wall. For the practical limit of six terms suggested in reference 2, both desirable flow characteristics cannot be achieved simultaneously. In view of earlier considerations in selecting control points A and B (fig. 4), a Thwaites' solution for a bounding streamline through these points should result in a monotonically increasing velocity in this region. Therefore, the choice of conditions for evaluating the coefficients was made which insures as uniform a velocity as possible at the entrance (x = −L). For six terms of the series (N = 6) and an arbitrary choice of $a_1 = 1$,

$$a_k = C_k \frac{I_1\left[\frac{\pi}{L} R(-L)\right]}{I_1\left[k \frac{\pi}{L} R(-L)\right]}; \quad k = 2,3,\cdots 6$$

where $C_2 = 5/4, C_3 = 5/6, C_4 = 1/3, C_5 = 5/54$, and $C_6 = 7/324$.

This choice of coefficients usually results in a small adverse velocity gradient at the entrance which might cause separation. However, as will be seen later, in this application, the adverse gradient was avoided.

The stream function is constant along streamlines. Hence, a_o is evaluated by equating values of the stream function at both ends of the bounding streamline, i.e., ψ for $x = 0, r = R(0)$ is equated to ψ for $x = -L, r = R(-L)$. It is then possible to evaluate ψ along the bounding streamline, ψ_{bs}.

The coordinates of the bounding streamline, R(x), are found as solutions to

$$\psi_{bs} = \frac{1}{2} a_o^2 \left(\frac{\pi R}{L}\right)^2 + \left(\frac{\pi R}{L}\right) \sum_{k=1}^{6} \frac{a_k}{k} \cos\left(k \frac{\pi x}{L}\right) I_1\left(k \frac{\pi R}{L}\right) \tag{5}$$

with $-L \leq x \leq 0$ specified. This method of solution was programmed and solved on an IBM 360/67 computer.

The first attempt to obtain the bounding streamline used the actual settling-chamber radius, equivalent test section radius (based on cross-sectional area) and predetermined L_{max}. The resulting solution, which does not pass through points A and B, is shown in figure 5 as solution 1. Subsequent attempts using successively shorter entrance-section lengths (L_{max}) were also unsuccessful because the curvature of the bounding streamline soon becomes so small near the entrance that the solution could not be found over the entire length using only six terms of the series.

An alternative approach was chosen. A fictitious length and entrance radius, smaller than the physical size, was used to find a solution which passed through A and B and only a portion of that solution was used with the remainder of the bounding streamline specified by practical physical constraints. Two such trial results are shown in figure 5 (solutions 2 and 3). Solution 3 passes through points A and B. The velocity along the bounding streamline was found to decrease slightly from the entrance to point D and then monotonically increase from point D to point A. At point C, where the streamline slope is minus one, the velocity increases to only about 10 percent of its final value. Therefore, the Thwaites' solution was used between points C and A and a 45° conical section, the dashed line in figure 5, was used ahead of point C to satisfy the physical constraints of L_{max} and settling-chamber radius.

With an area distribution now available for an axisymmetric entrance section, the next step is to devise a scheme to permit smooth transition of the flow from the circular-cross-section settling chamber to the rectangular test section.

Transition from Circular to Rectangular Cross Section

The length defined by points C and A in figure 5 was selected for making the transition from circular to rectangular cross section. This choice was made since about 90 percent of the total velocity increase occurs in this length and since construction is simplified by mating the transition section with adjoining sections of constant slope. The complete entrance section, thus defined, is shown in figure 6.

The area distribution in the transition section is given by (see fig. 6)

$$A(x) = \pi R^2(x) = w(x)h(x) - (4 - \pi)\, r_c^2(x) \; ; \quad x_1 \leq x \leq 0 \tag{6}$$

R(x), dR(x)/dx, w(0), and h(0), and $r_c(0)$ are given. The corner radius at the test section entrance, $r_c(0)$, need not be zero. In fact, it was found that for fixed values of w(0) and h(0), the degree of smoothness of the transition at the high-velocity end is dependent critically upon the value of $r_c(0)$. The final choice of values for w(0), h(0), and $r_c(0)$ determines the value of R(0) used in the Thwaites' solution (see eq. (6) for x = 0).

The side walls of the transition are described by a five-term polynomial whose coefficients are determined by satisfying five boundary conditions. For example, for the half height

$$h(x)/2 = h_0 + h_1 x + h_2 x^2 + h_i x^i + h_j x^j \; ; \quad x_1 \leq x \leq 0 \tag{7}$$

with boundary conditions

$$\left.\begin{aligned}
&1.\ \text{at } x = 0 \quad h(x)/2 = h(0)/2 \\
&2.\ \text{at } x = 0 \quad \frac{dh(x)/2}{dx} = 0 \\
&3.\ \text{at } x = x_1 \quad h(x)/2 = R(x_1) \\
&4.\ \text{at } x = x_1 \quad \frac{dh(x)/2}{dx} = \frac{dR(x)}{dx}\bigg|_{x_1} \\
&5.\ \text{at } x = x_1 \quad \frac{d^2h(x)/2}{dx^2} = 0
\end{aligned}\right\} \tag{8}$$

Boundary condition 5 is imposed to insure that h(x)/2 varies monotonically. The exponents of the last two terms of eq. (7) are generalized as i and j so they may be changed to improve the degree of

smoothness of the walls and minimize the deviation of h(x)/2 from R(x). Application of the boundary conditions, eqs. (8), yields for the coefficients of eq. (7).

$$
\left.
\begin{aligned}
h_0 &= h(0)/2 \\
h_1 &= 0 \\
h_2 &= \frac{ij[(i-1)(j-2)-(i-2)(j-1)][2R(x_1)-h(0)]}{(i-2)(j-i)(j-2)x_1^2} \\
&\quad + \frac{[(i+1)(i-2)j(j-1)-i(i-1)(j+1)(j-2)]x_1 \left.\frac{dR(x)}{dx}\right|_{x_1}}{(i-2)(j-i)(j-2)x_1^2} \\
h_i &= 2\left\{\frac{-j[2R(x_1)-h(0)]+(j+1)x_1 \left.\frac{dR(x)}{dx}\right|_{x_1}}{(i-2)(j-i)x_1^i}\right\} \\
h_j &= 2\left\{\frac{i[2R(x_1)-h(0)]-(i+1)x_1 \left.\frac{dR(x)}{dx}\right|_{x_1}}{(j-2)(j-i)x_1^j}\right\}
\end{aligned}
\right\} \qquad (9)
$$

Note from the denominators of eqs. (9) that i must be greater than 2 and $j > i$. Similar expressions for the half width are obtained by replacing h by w and i, j by m, n, respectively, in eqs. (7) through (9).

Finally, the corner radius distribution, $r_c(x)$, is determined from eq. (6). The entire transition procedure was programmed for the IBM 360/67 computer and combined with the programmed solution of Thwaites.

PILOT FACILITY AND TESTS

The above method was used to design the entrance section for a High Reynolds Number Channel at the Ames Research Center. To determine that the method does, in fact, provide smooth transition of the flow from a circular to a rectangular cross section, a 0.4-scale model of the entrance section and half of the test-section length of the actual channel was built and tested. This model is subsequently referred to as the pilot facility.

Computer inputs used to design the transition section of the pilot facility (after several iterations) are given in table 1. The resulting axisymmetric radius distribution for the transition section is tabulated in table 2 and plotted in figure 7. Also shown in figure 7 are the distributions w(x)/2, h(x)/2, and $r_c(x)/2$.

Facility

A photograph of the pilot facility is shown in figure 8. The downstream end of the test section is mounted on a gate valve, which, in turn, is mounted on a vacuum chamber. Figure 9 is a sketch showing the pertinent details of the pilot facility. At station $x = 0$, the corner radius of the entrance section is $r_c(0) = 0.762$ cm. To facilitate construction of the test section, the corners were wedge shaped as indicated in figure 9. The wedges were sized to provide the same cross-sectional area had corner radii been used. This required some hand fairing at, and downstream of, station $x = 0$.

Locations of static-pressure orifices are also indicated in figure 9. The orifices in the transition section and the top and bottom walls of the test section were permanent. Eight orifices were located circumferentially in the transition cross section only at $x = -10.16$ and -22.86 cm. At all other negative x-stations, orifices were located at only the top, side, and radius location of one quadrant. The orifices in the side walls of the test section were mounted in removable plugs which could be replaced with a pressure-survey probe that completely spanned the test section. The probe orifice was 5.24-cm ahead of the probe support.

The nominal free-stream Mach number was controlled by choke inserts (of appropriate thickness) at the downstream end of the test section (see fig. 9).

Tests

Tests were made at atmospheric total pressure for free-stream test-section nominal Mach numbers of 0.6, 0.7, 0.8, and 0.9. Static and total pressure surveys were made, one location at a time, with separate probes rather than with a pitot-static probe. The probes were specially designed to minimize errors due to compressibility effects (local shock waves) at the higher Mach numbers.

Pressures where sensed by a standard pressure transducer used in conjunction with a "scanivalve." The output signal from each orifice was recorded on magnetic tape and a computer program was used to convert the records to absolute pressure. The ratios of static to total pressures were used to obtain Mach number as indicated in reference 4.

Because the full-scale facility employs screens in the stagnation chamber (see fig. 2) most of the data were obtained with a screen over the entrance section. To evaluate the effects of the screen, data were also obtained with no screen.

A minimum number of tests were made using a surface oil-flow technique to establish local flow direction and demonstrate the lack, or existence, of secondary flows near the walls (boundary-layer separation).

RESULTS AND DISCUSSION

Results are presented in a manner to evaluate the degree of uniformity of flow in the pilot facility. Longitudinal Mach number distributions are presented for the complete facility (entrance section and test section); transverse distributions of Mach number in the test section are presented. Also presented are the results of total pressure surveys in the test section and oil-film studies which were made to determine the existence, if any, of secondary flows.

Mach Number Distributions

Longitudinal surveys – The Mach number distribution in the longitudinal direction (x) of the pilot facility is presented in figure 10 for test-section nominal free-stream Mach numbers, $M_{\infty,nom}$ of 0.6, 0.7, 0.8, and 0.9. The Mach numbers obtained from wall static pressures are shown by open symbols for the empty channel, and for the channel with the probe in its most downstream location (x = 19.84 cm, y = z = 0 cm). Each data point is the average of the Mach numbers calculated using pressures measured at several circumferential locations (see fig. (9)). The deviation of the individual circumferential values of Mach number from the average was, in the worst case, ±2 percent and in most cases was less than ±1 percent. The reduction in Mach number due to the blockage of the probe support is obvious. The filled symbols represent the Mach number determined from static pressure measurements at the centerline of the test section with the probe support at the x-station indicated. There is excellent agreement downstream of the test section entrance between the Mach numbers determined from stream- and wall-static pressure measurements with the probe support at x = 19.84 cm. The data show the existence of a longitudinal gradient in Mach number in the test section which is attributed to boundary-layer growth along the walls. (In the full-scale facility the top and bottom test-section walls are hinged upstream and designed as converging-diverging walls to provide a means for minimizing longitudinal gradients.) Comparing the experimental channel-empty data with the theoretical estimates using reference 4, it is seen that the agreement is much better at the lowest nominal Mach number and at the low-velocity end of the entrance section for all nominal Mach numbers. This is consistent with the fact that viscous effects become more significant as the Mach number and area ratio $A(x)/A^*$ (A^* is the throat area) approach unity.

Transverse surveys – Typical distributions of Mach number in the test section in planes normal to the channel longitudinal axis are presented in figures 11 through 14. Figure 11 shows the distributions at the test-section entrance (x = 0) for the free-stream nominal Mach number, $M_{\infty,nom} = 0.8$. These data show a higher velocity at the walls than at the centerline. Any reasonable estimate from these data of an average Mach number at the walls would be greater than that indicated by the faired curve through the square open-symbol data at x = 0 in figure 10(c). This suggests the possibility of a slight adverse pressure gradient at the beginning of the test section, but if this was the case, the magnitude of the gradient was not sufficient to cause boundary-layer separation or induce secondary flows downstream (as noted later).

The higher velocity at the wall compared to the centerline at the entrance of the test section is also indicated theoretically by the finite-length axisymmetric solution of Thwaites (also see fig. 3(b)). The ratio of the velocity obtained from the Thwaites' solution across the exit of the axisymmetric entrance to that at the centerline is shown in figure 12. (Note the expanded scales.)

Also shown is the Mach number ratio across the test-section entrance in the y and z directions from figure 11. These data indicate that the flow is less uniform across the test-section entrance in the horizontal direction (short dimension) than that indicated for an axisymmetric channel, and more uniform in the vertical direction (long dimension).

The data demonstrate a slight asymmetry (skewness) of the flow, about 1.5 percent in the y direction and less than 0.5 percent in the z-direction. The asymmetries were determined to result from asymmetries inadvertently built into the entrance section. This fact was established by tests made with the entire pilot facility rotated 180°. The results are shown in figure 13.

The horizontal distributions of Mach number across the center of the test section (z = 0) at stations downstream of x = 0 are shown in figure 14 for several values of M_{-nom}. The data demonstrate completely uniform flow across the test section at these locations. This is the reason for the excellent agreement between the Mach numbers at these x-locations determined from wall and stream static pressures noted earlier (figure 10).

Total Pressure Distributions and Oil-Flow Patterns

To determine the possible existence of secondary flows, total pressure measurements were made at the same (and more) locations in the test section for which free-stream static pressure measurements were made. The surveys were made to within 0.32 cm of the side walls and 0.49 cm of top and bottom walls. The results indicated no vortices in the flow and no boundary-layer separation at any free-stream Mach number. The only losses in total pressure recorded were a small drag-loss due to the screen and losses near the walls of the test section in the region of the boundary layer. The losses for $M_{-nom} = 0.8$ are shown in figure 15 as the ratio of total pressure measured in the test section to atmospheric total pressure. The scale on the right in figure 15 is included to emphasize the small magnitude of the total-pressure losses as a fraction of a percent of the local free-stream dynamic pressure.

Flow studies were made using an oil-film technique to establish the direction of the streamlines of the flow near the walls and to determine the presence, if any, of boundary-layer separation. Residual oil patterns indicated smooth flow (gently curving and straight streaks in the oil patterns) throughout the pilot facility with no apparent regions of boundary-layer separation. Photographs of typical oil-flow patterns are shown in figure 16. Figure 16(a) is a view into the entrance section and along the top and left-hand wall of the test section. Figure 16(b) is a view of the left-hand wall near the beginning of the Mach number choke inserts (small vertical white line at top center of photograph). The larger white streaks near the top of the photograph are localized regions of separated flow which are traceable to discrete imperfections in the surface fairing at the juncture of the entrance and test sections and are believed not to be the result of any adverse pressure gradient upstream along the walls (see fig. 16(a) at upper left-hand corner of juncture).

CONCLUDING REMARKS

A method has been presented for the design of entrance sections for high-speed subsonic wind tunnels with rectangular test sections. The technique includes a mathematical procedure for shaping an entrance section of specified length to insure a smooth transition of the flow from the circular cross section of a settling chamber to a rectangular test section. The technique was used to design the entrance section for the High Reynolds Number Channel at the Ames Research Center. A 40-percent scale model of the entrance section and part of the test section of this facility was built and tested to assess the design method and evaluate the flow in the test section. Initial results of surface static-pressure measurements in the entrance section, static- and total-pressure surveys in the test section and oil-flow patterns on all surfaces indicate that a uniform flow is attained downstream in the rectangular test section. No vortices were detected in the flow and no boundary-layer separation was detected.

REFERENCES

1. Tsien, Hsue-Shen: On the Design of the Contraction Cone for Wind Tunnel Feb. 1943, pp. 68 70

2. Thwaites, B. A.: On the Design of Contractions for Wind Tunnels. National Physical Laboratory, R. & M. 2278. March 1946.

3. Gothert, B.: Plane and Three-Dimensional Flow at High Subsonic Speeds. NACA TM - 1105, 1946.

4. Ames Research Staff: Equations, Tables, and Charts for Compressible Flow. NACA Rep. 1135, 1953.

TABLE 1.– COMPUTER INPUTS FOR TRANSITION-SECTION DESIGN

w(0)	10.16 cm
h(0)	15.24 cm
$r_c(0)$	0.762 cm
L(fictitious)	61 cm
R(−L) (fictitious)	30.5 cm
$\left.\frac{dR(x)}{dx}\right\|_{x_1}$	−1.0
i, j	11, 13
m, n	6, 7

TABLE 2.– AXISYMMETRIC ENTRANCE SECTION (TRANSITION REGION)

−x, cm	R(x), cm
0.0	7.01
1.02	7.02
2.03	7.03
3.05	7 06
4.06	7.10
5.08	7.16
6.10	7.22
7.11	7.30
8 13	7.39
9.14	7.50
10.16	7.62
11.18	7 75
12.19	7.90
13.21	8.06
14.22	8.24
15.24	8.44
16.26	8.66
17.27	8.89
18.29	9.15
19.30	9.43
20.32	9.73
21.34	10.06
22.35	10.41
23.37	10.79
24.38	11.21
25.40	11.66
26.42	12.14
27.43	12.67
28.45	13.24
29.46	13.86
30.48	14.54
31.50	15.28
32.51	16.10
33.53	17.00
34.15	17.60

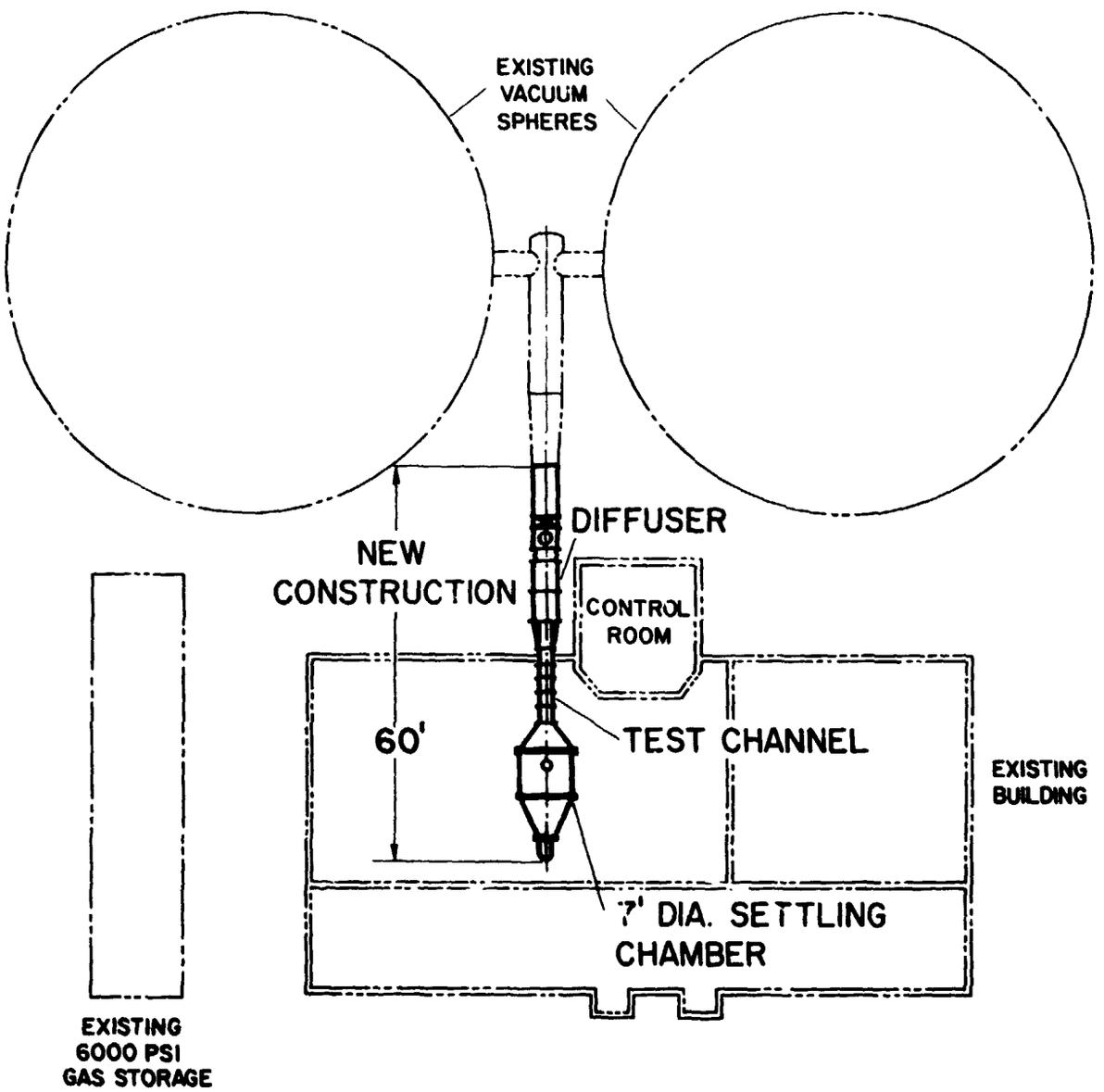

Figure 1.– Schematic of High Reynolds Number Channel facility.

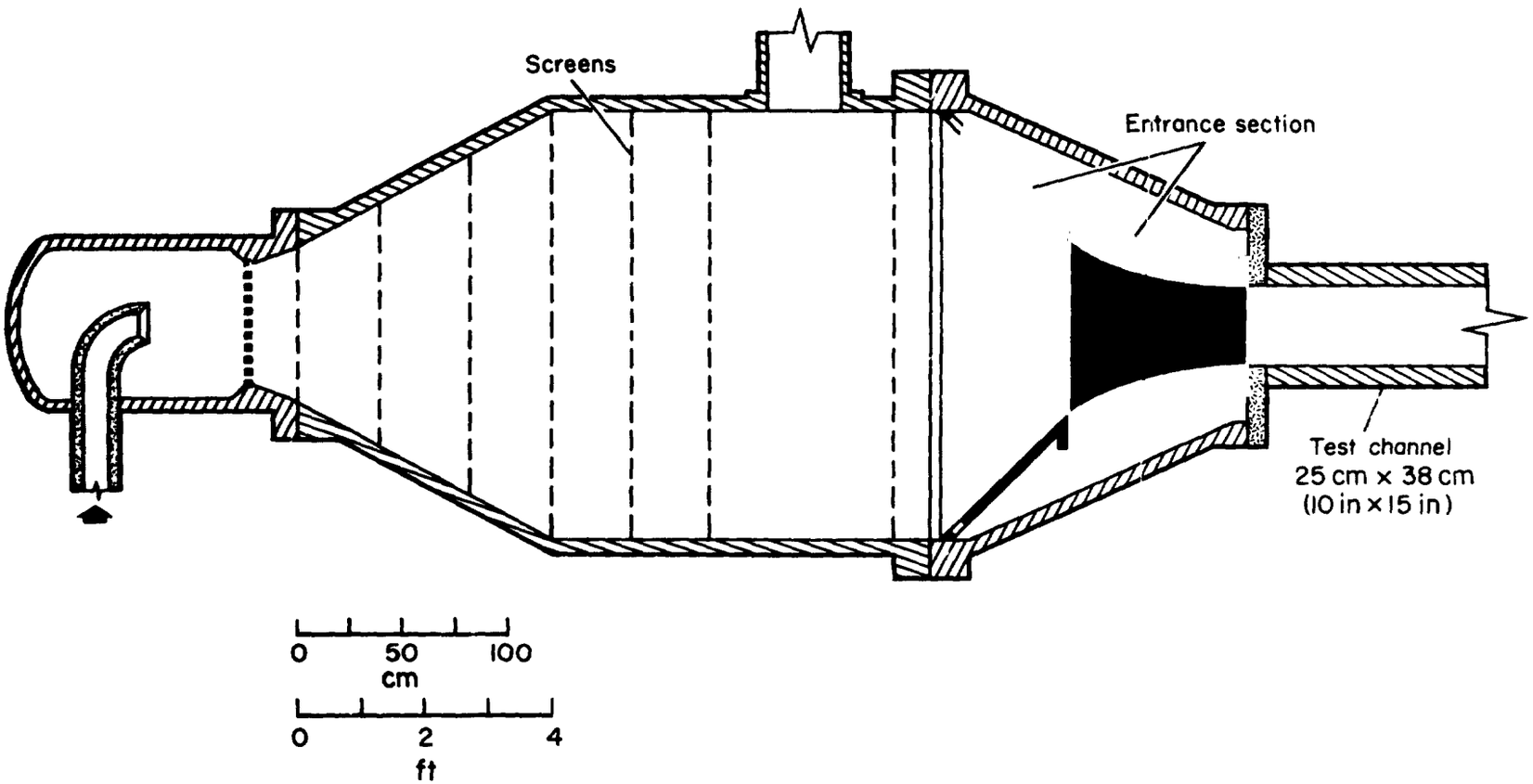

Figure 2. – Schematic of the settling chamber and entrance section for the Ames High Reynolds Number Channel facility.

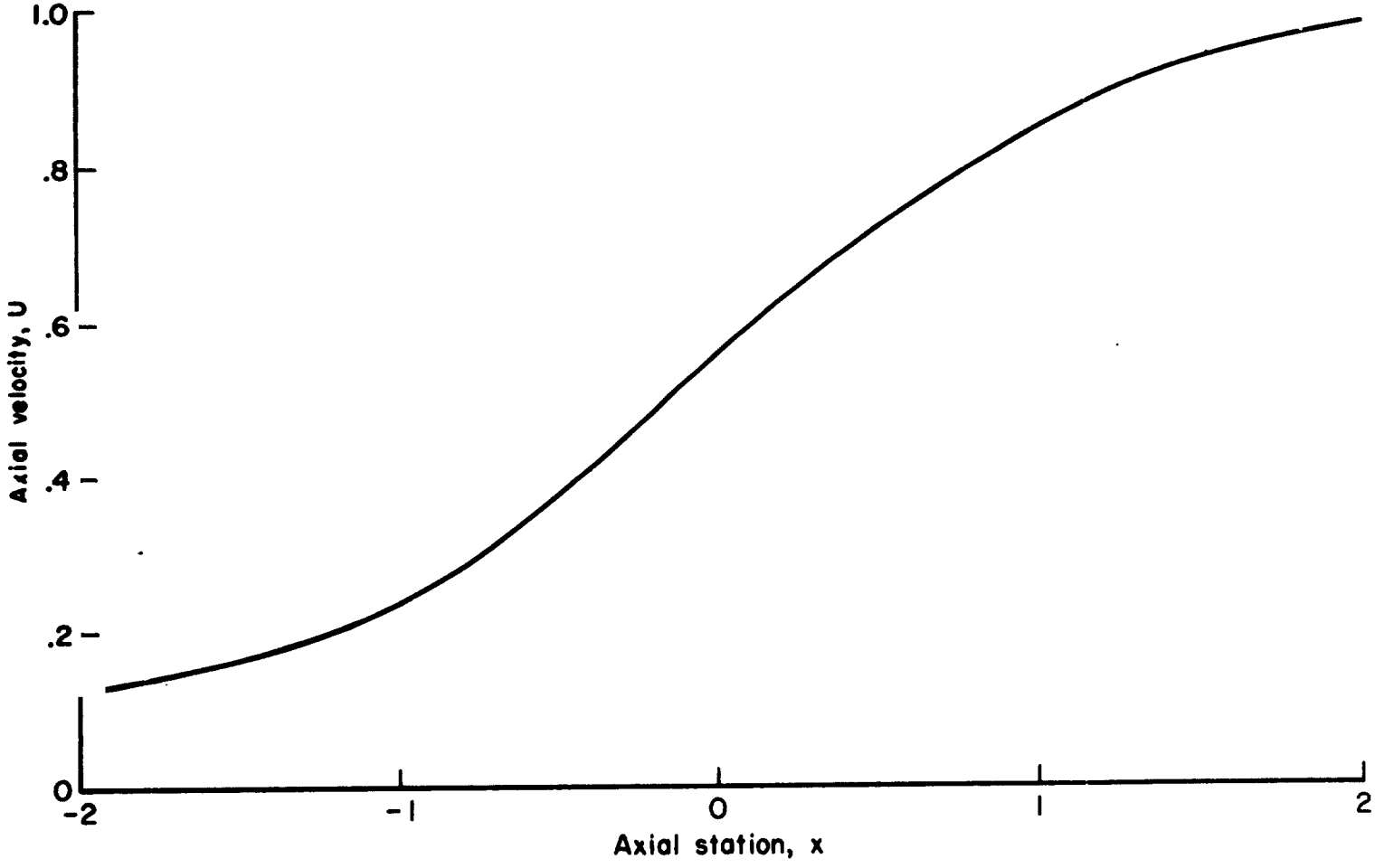

(a) Specified velocity distribution

Figure 3. – Results from Tsien's method for designing contraction cones (Ref. 1).

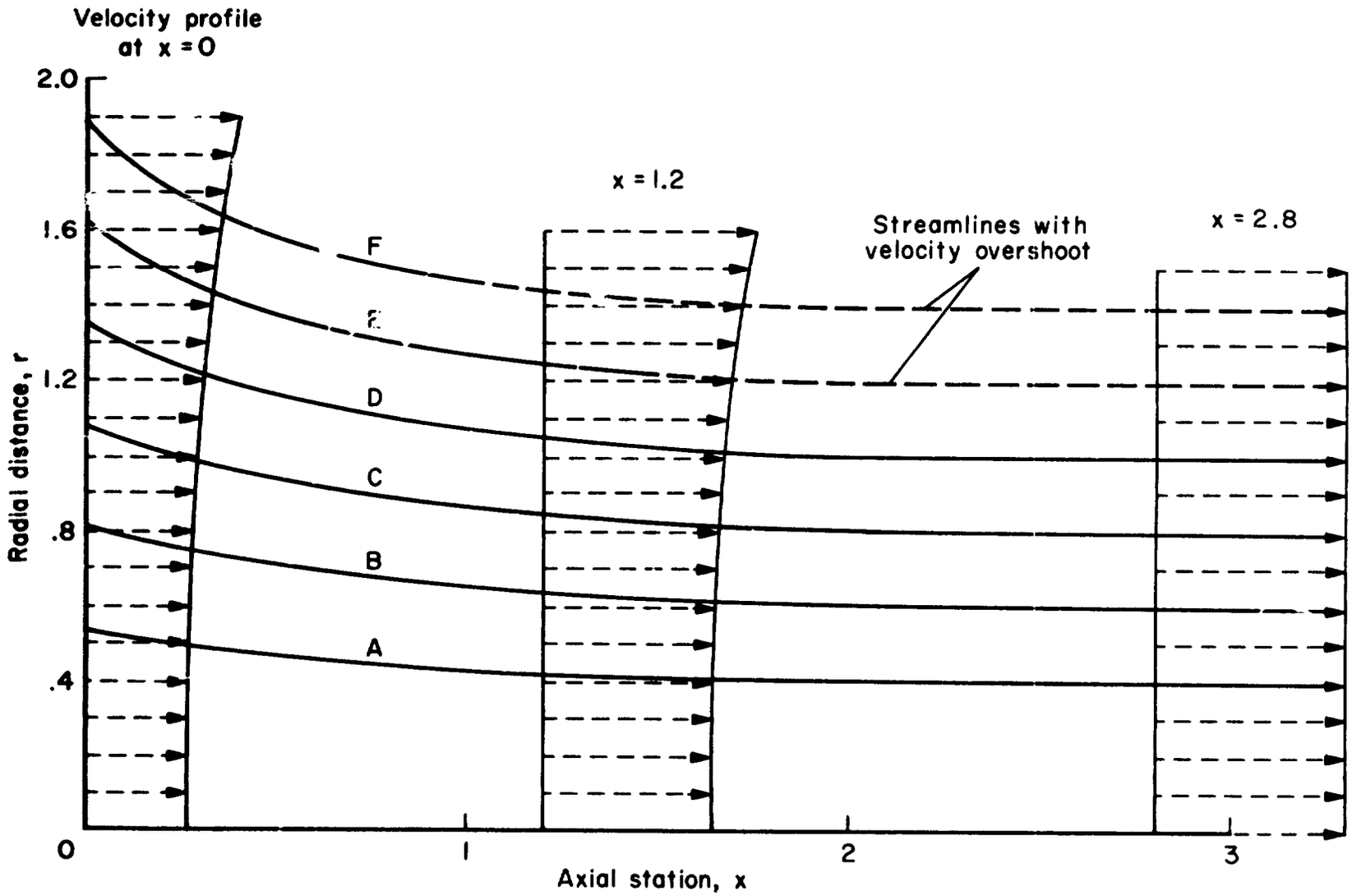

(b) Streamlines and velocity profiles

Figure 3.— Concluded.

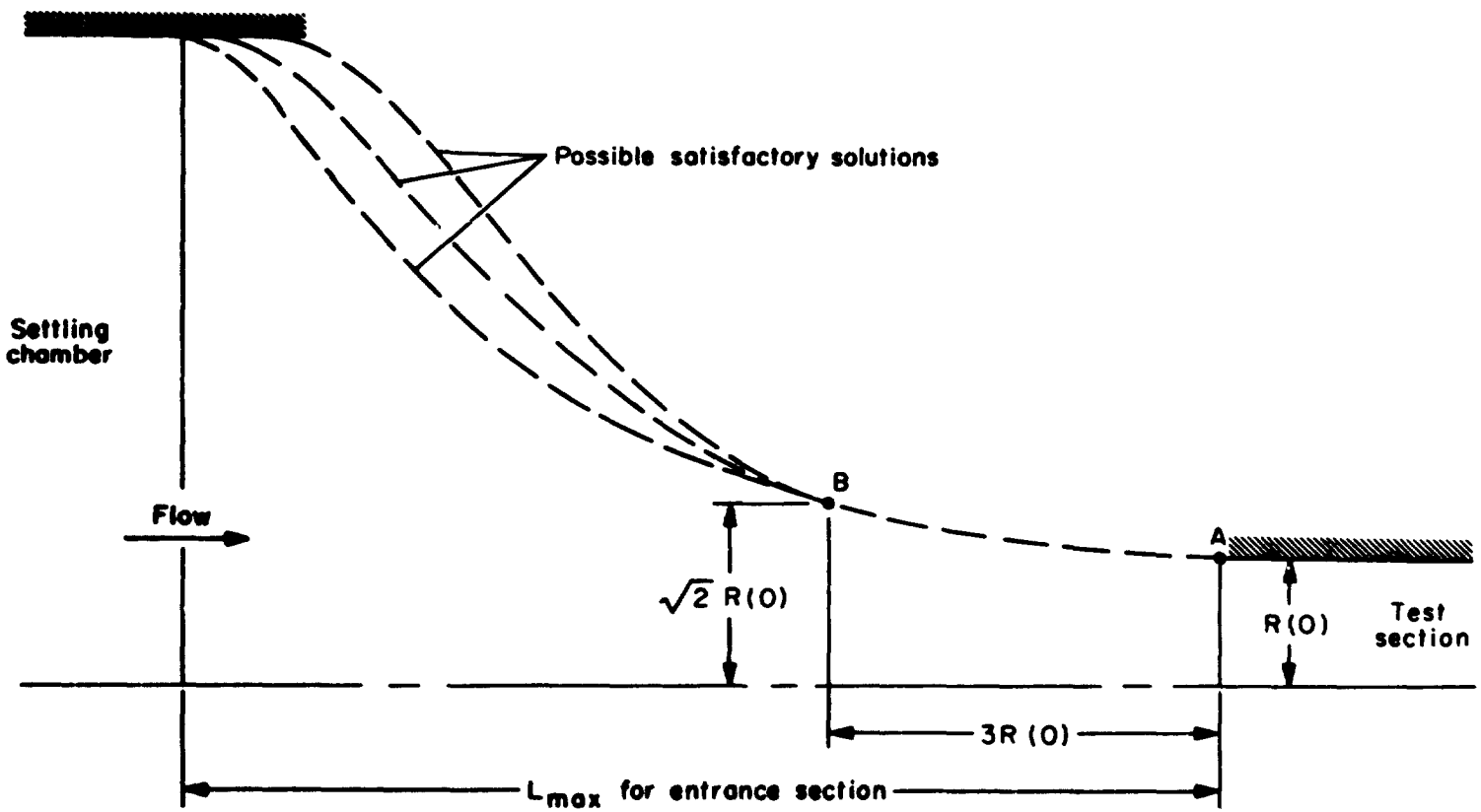

Figure 4. – Entrance section control points from Tsien's axisymmetric solution.

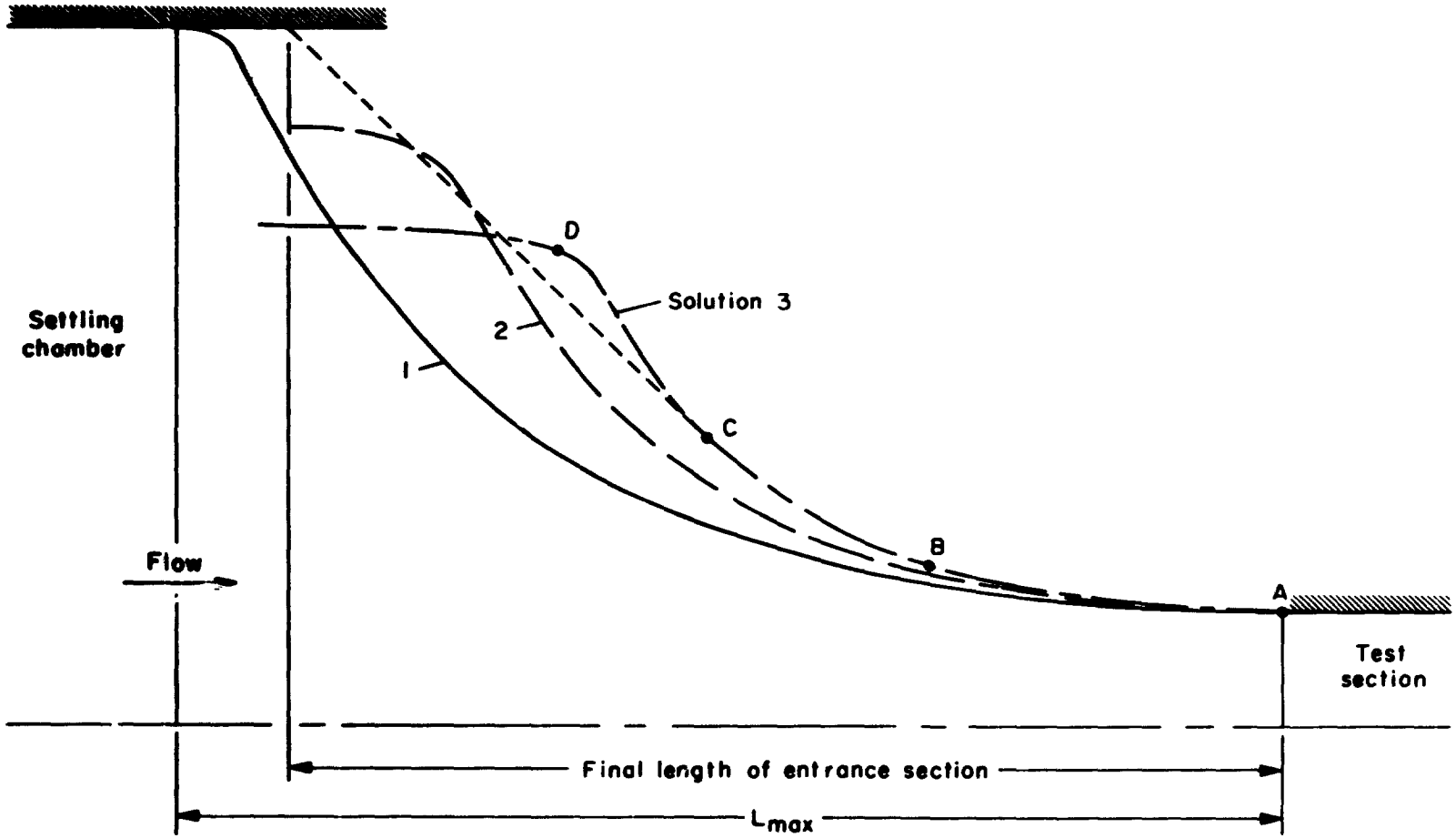

Figure 5. – Thwaites solutions for bounding streamlines near and through control points A and B.

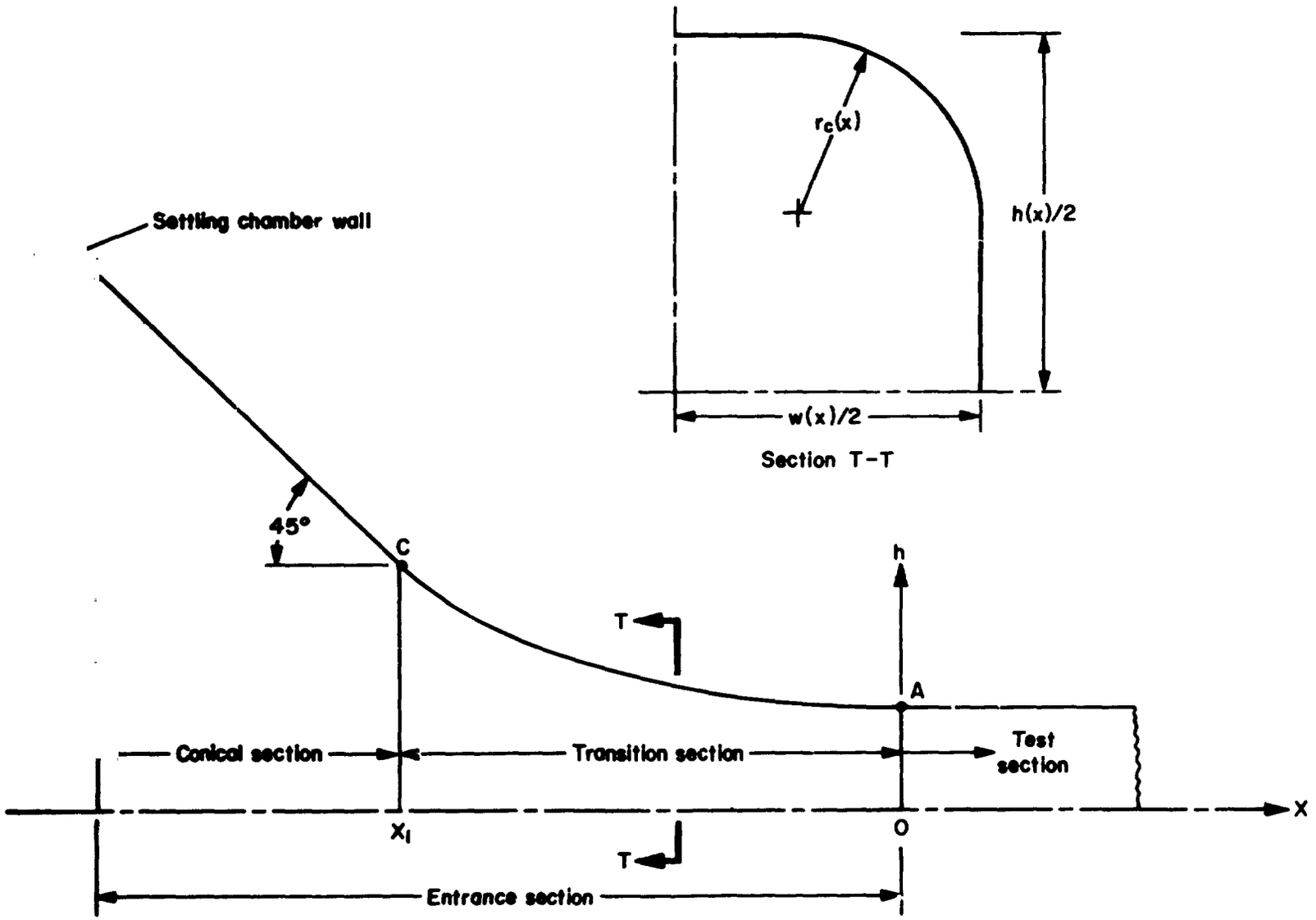

Figure 6. - Schematics of entrance section

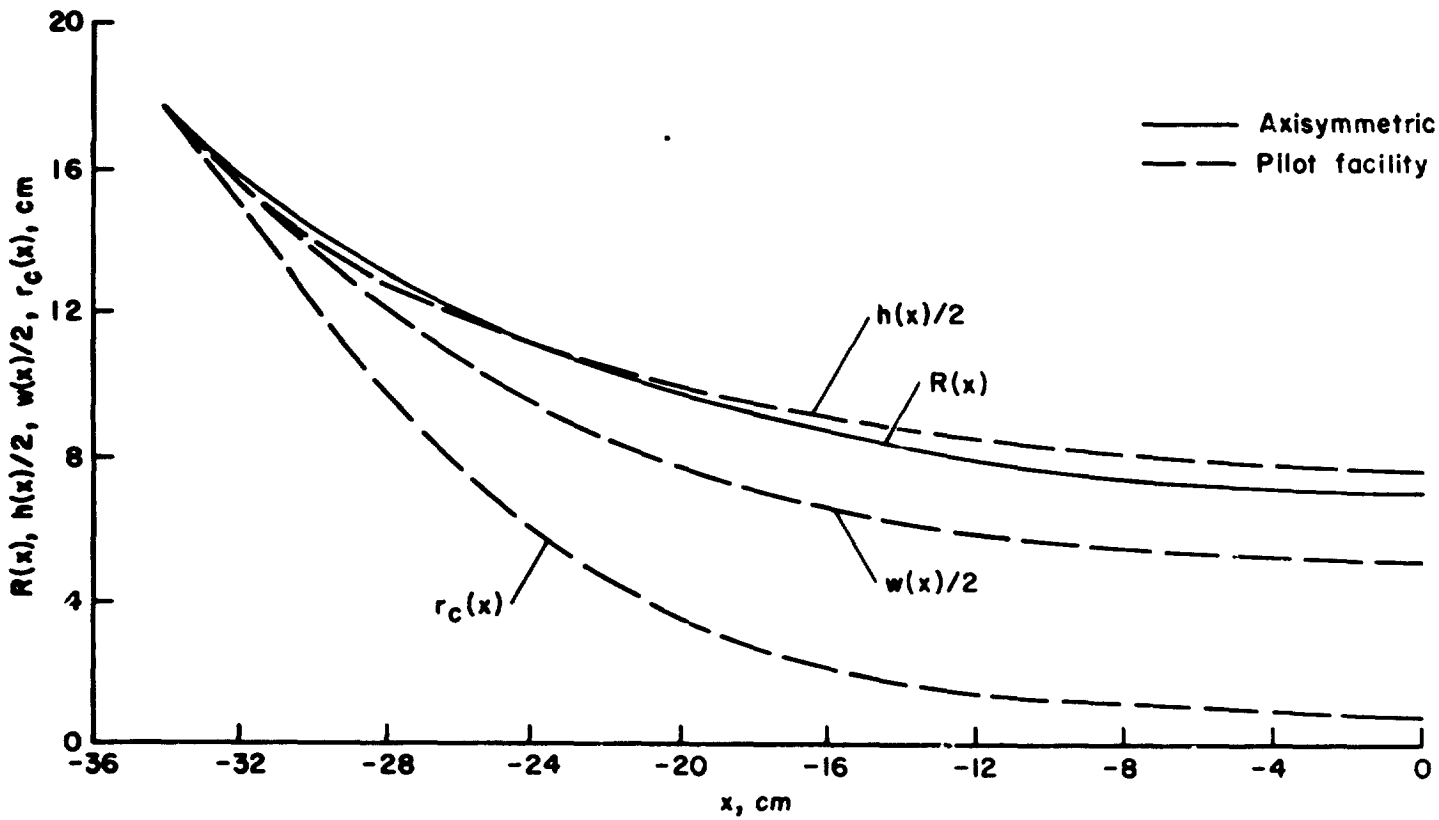

Figure 7. Dimensions of transition section for axisymmetric channel and pilot facility.

Figure 8. Photograph of the pilot facility for the High Reynolds Number Channel.

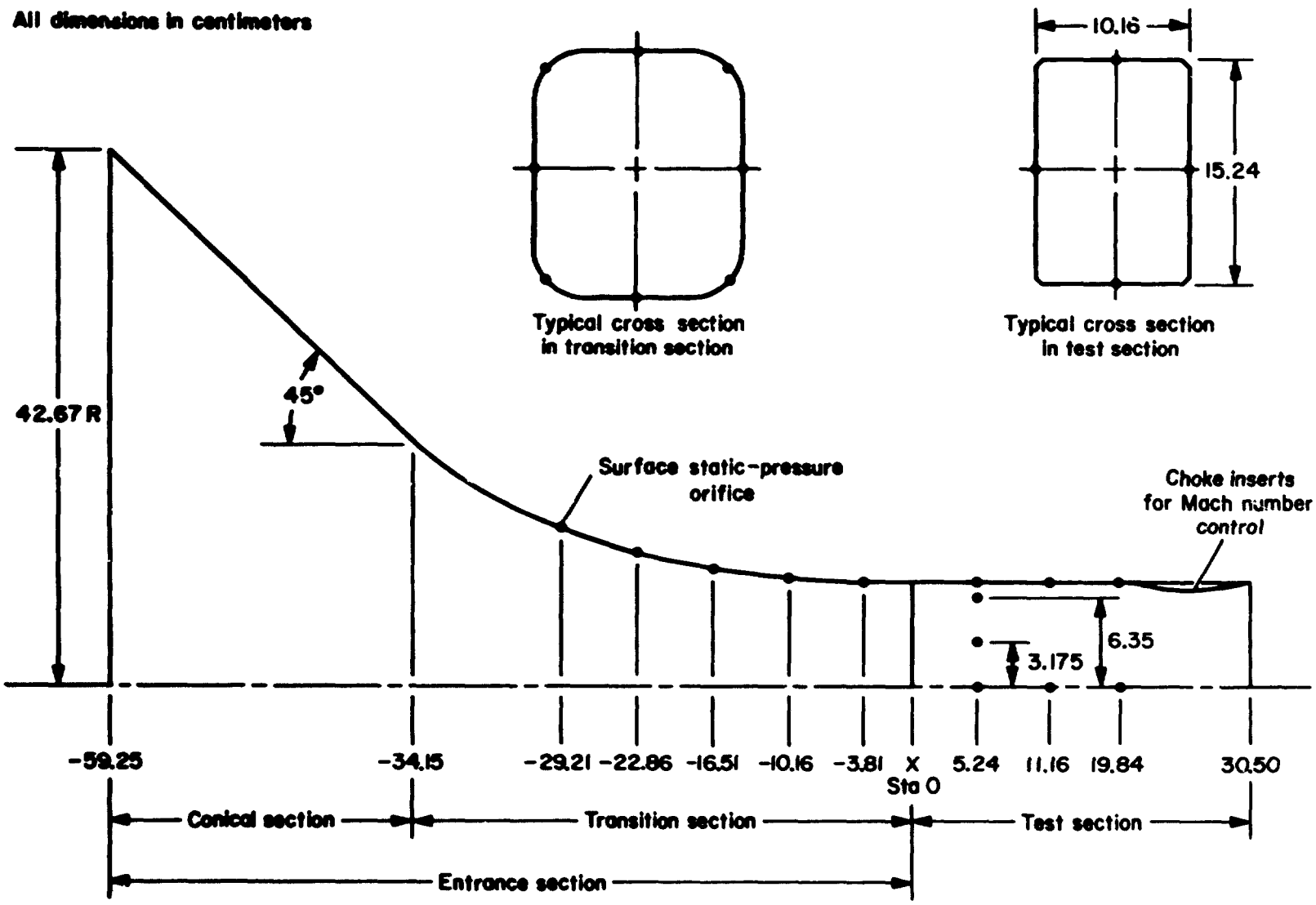

Figure 9. Sketch showing pertinent details of pilot facility.

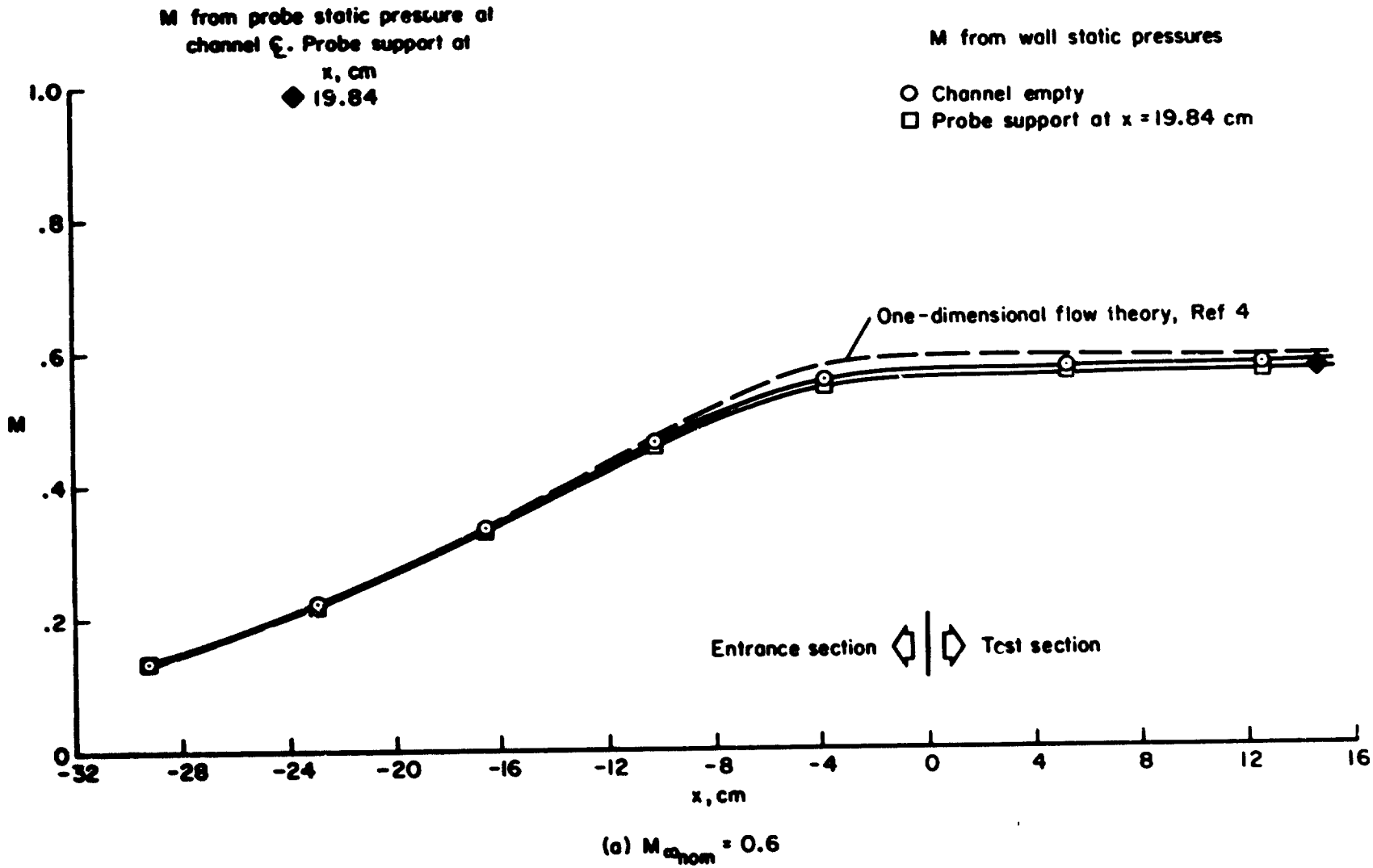

(a) $M_{\infty_{nom}} = 0.6$

Figure 10. – Longitudinal Mach number distribution in pilot facility.

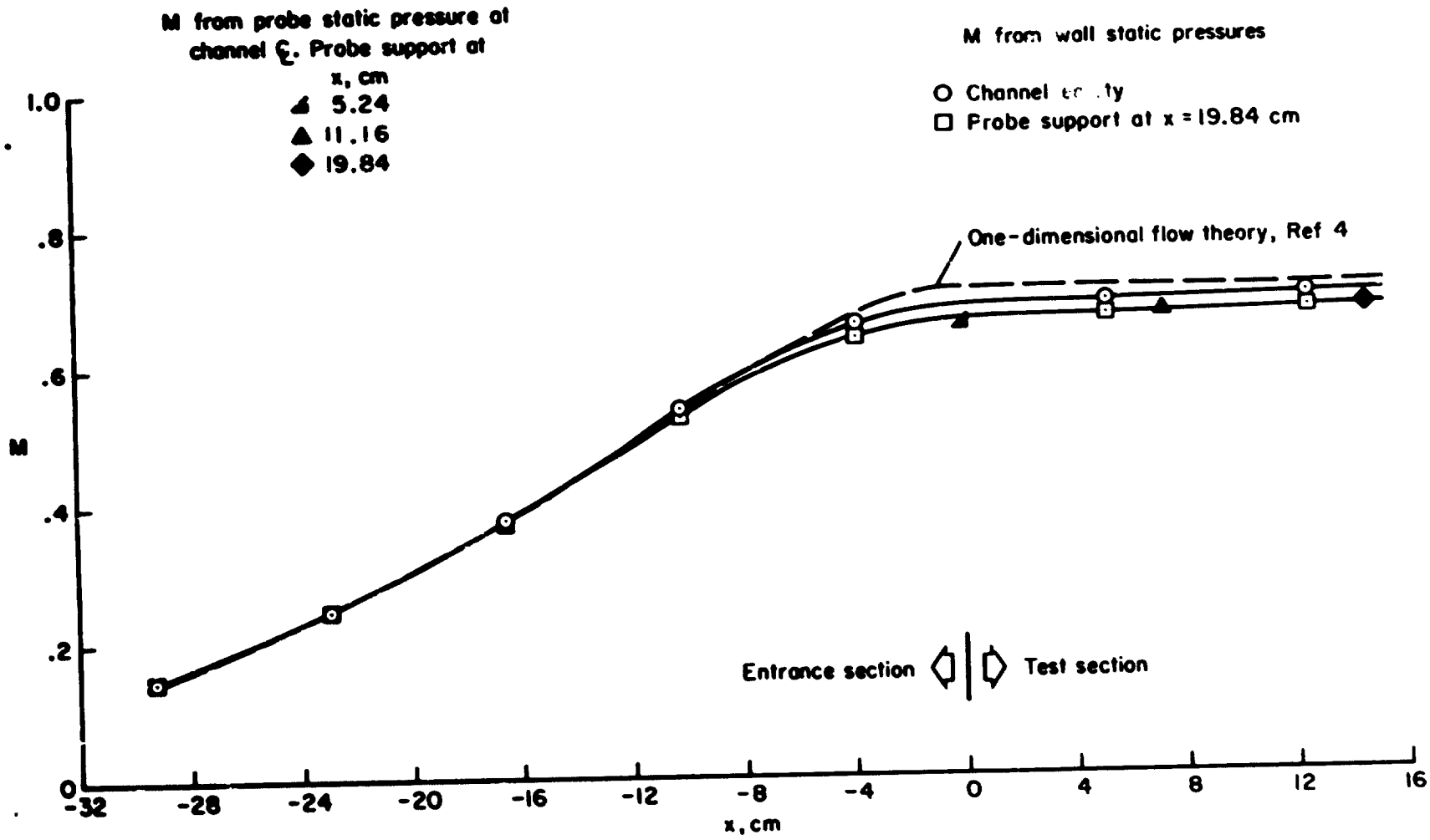

(b) $M_{\infty_{nom}} = 0.7$

Figure 10. - Continued.

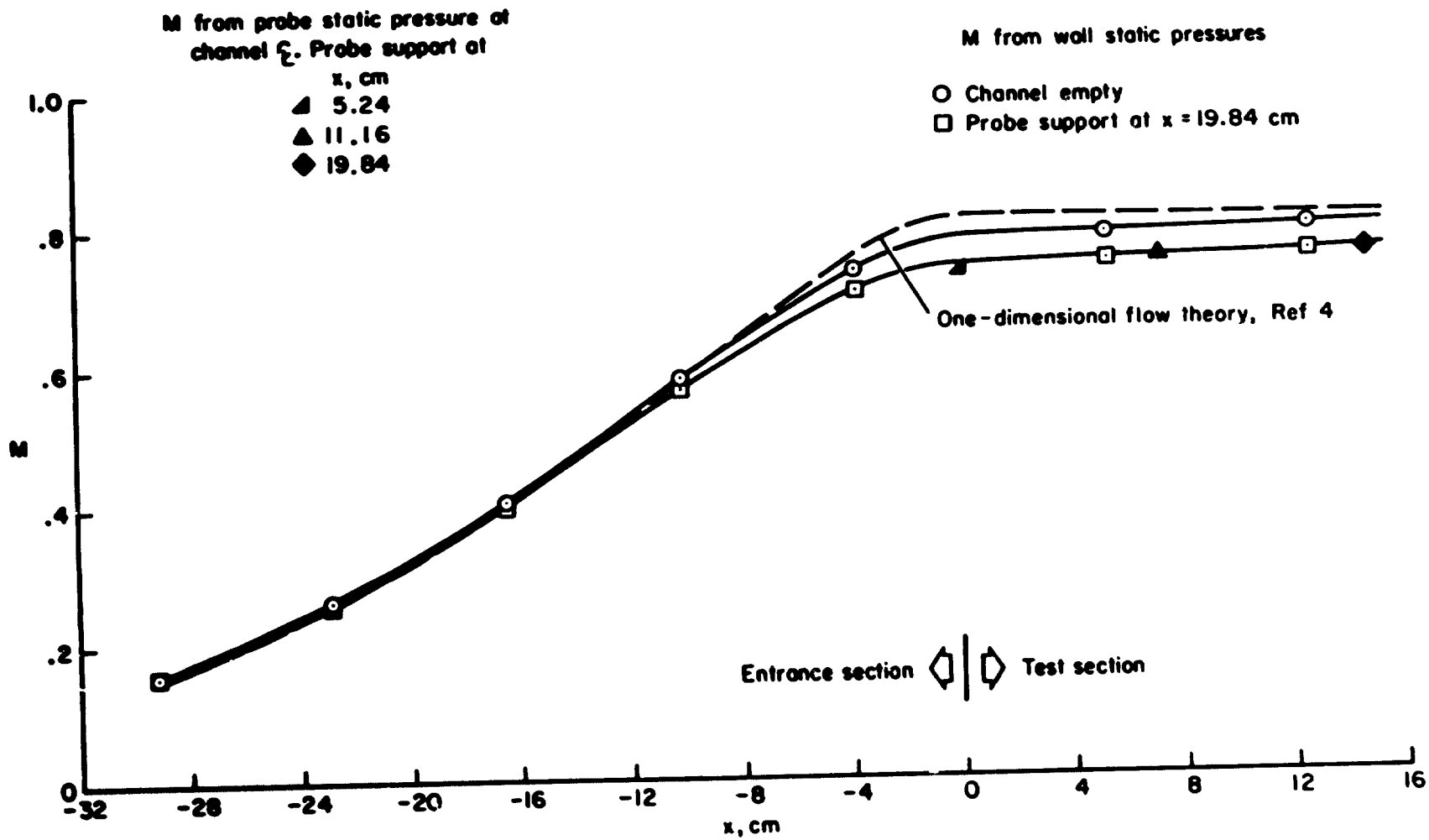

(c) $M_{\infty_{nom}} = 0.8$

Figure 10. – Continued.

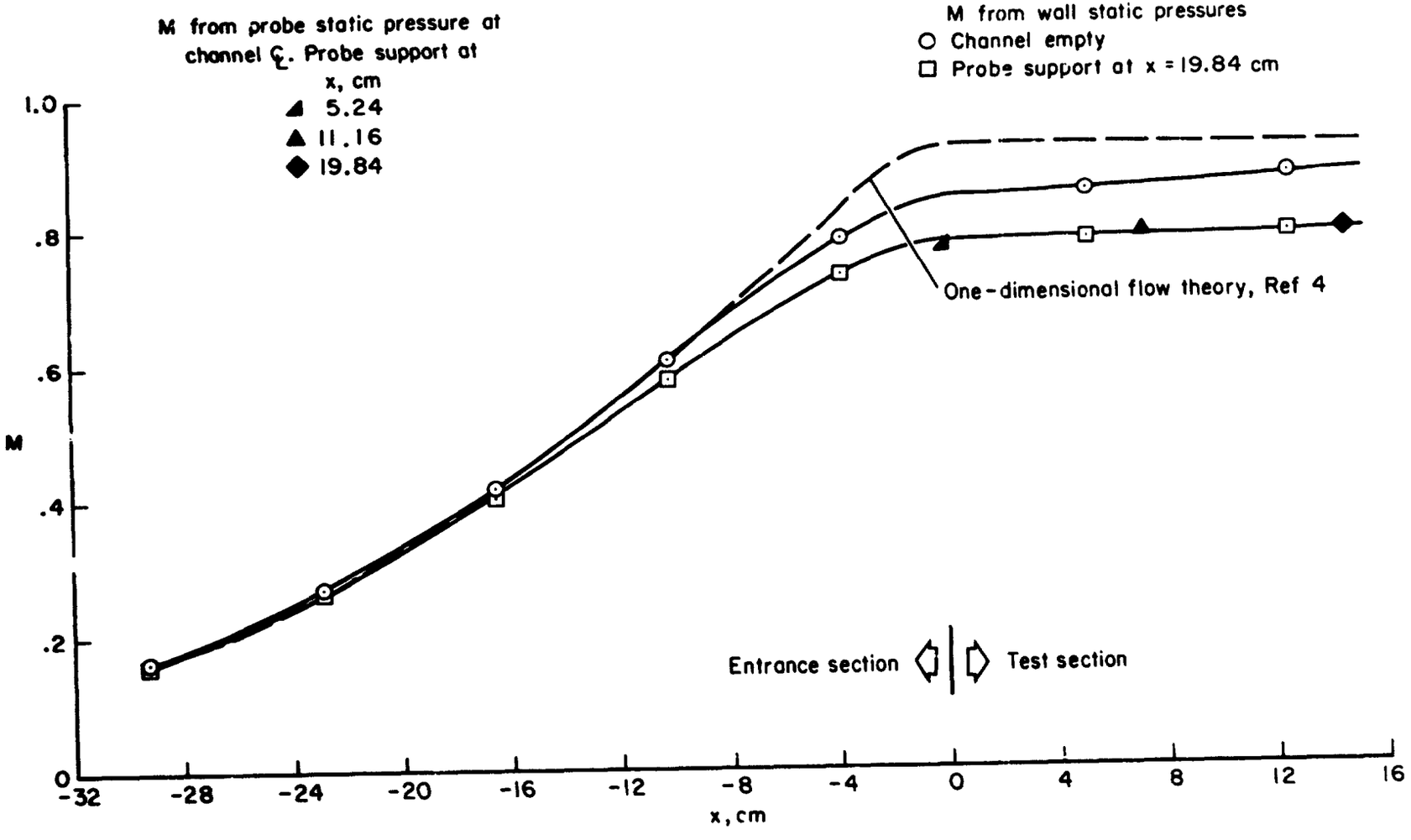

(d) $M_{\infty_{nom}} = 0.9$

Figure 10. – Concluded.

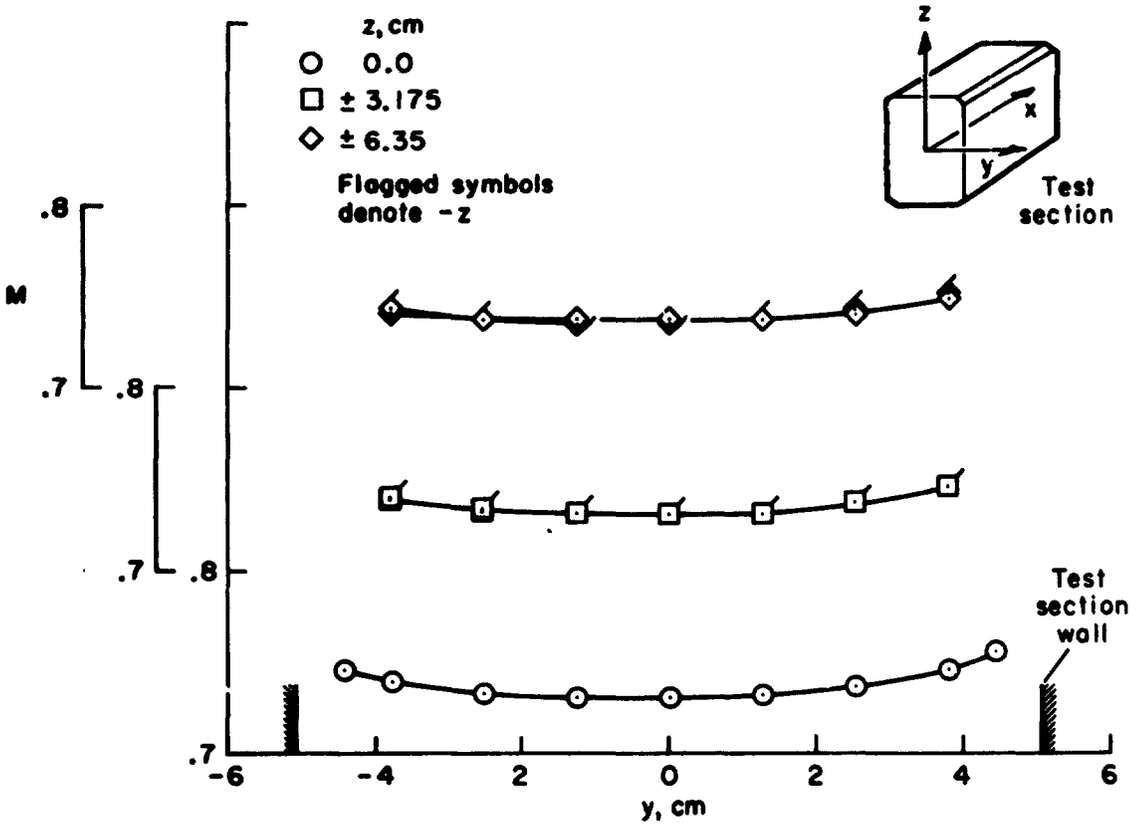

(a) Horizontal surveys

Figure 11. – Transverse Mach number distributions at test-section entrance (x = 0 cm) for $M_{nom} = 0.8$.

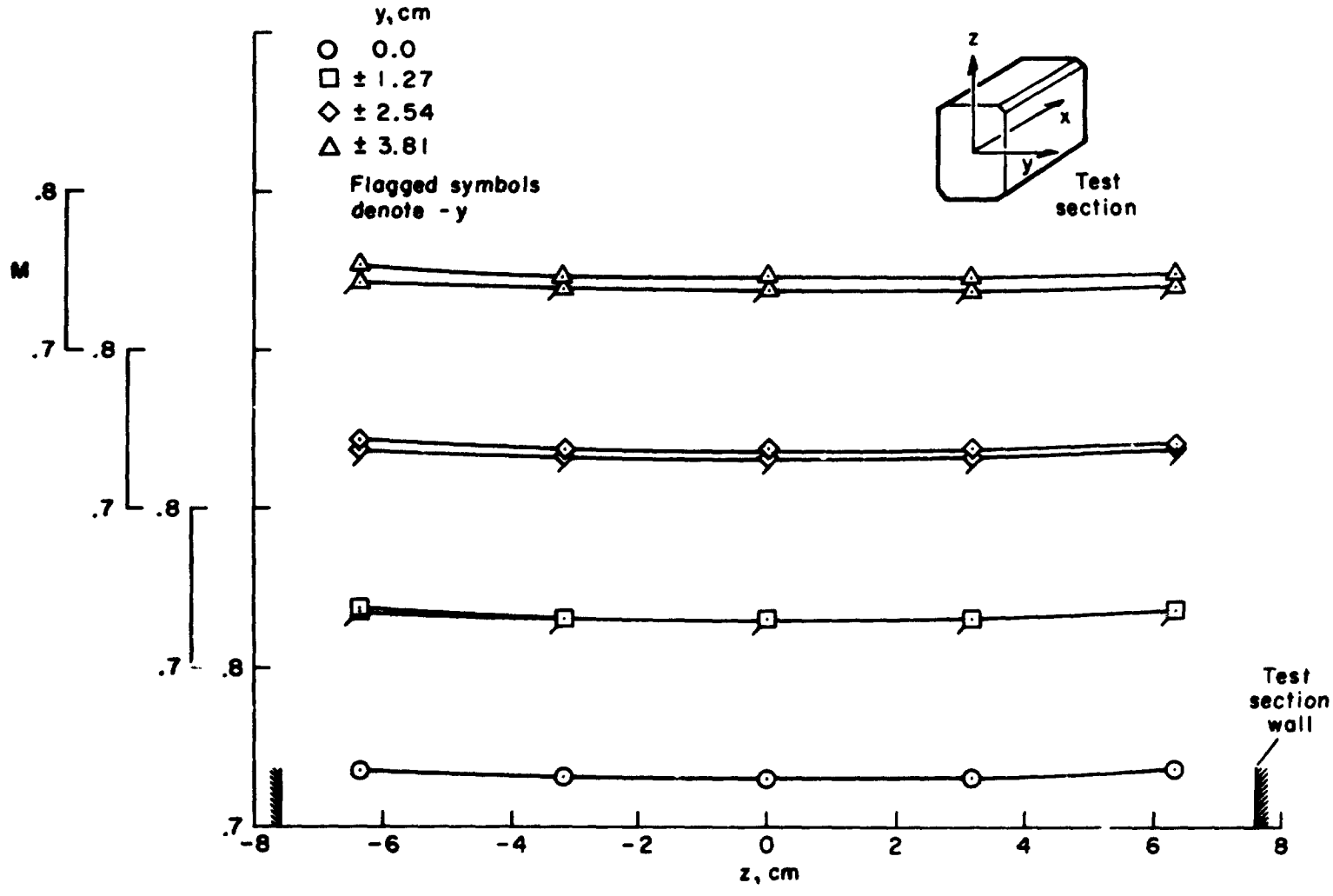

(b) Vertical surveys

Figure 11.– Concluded.

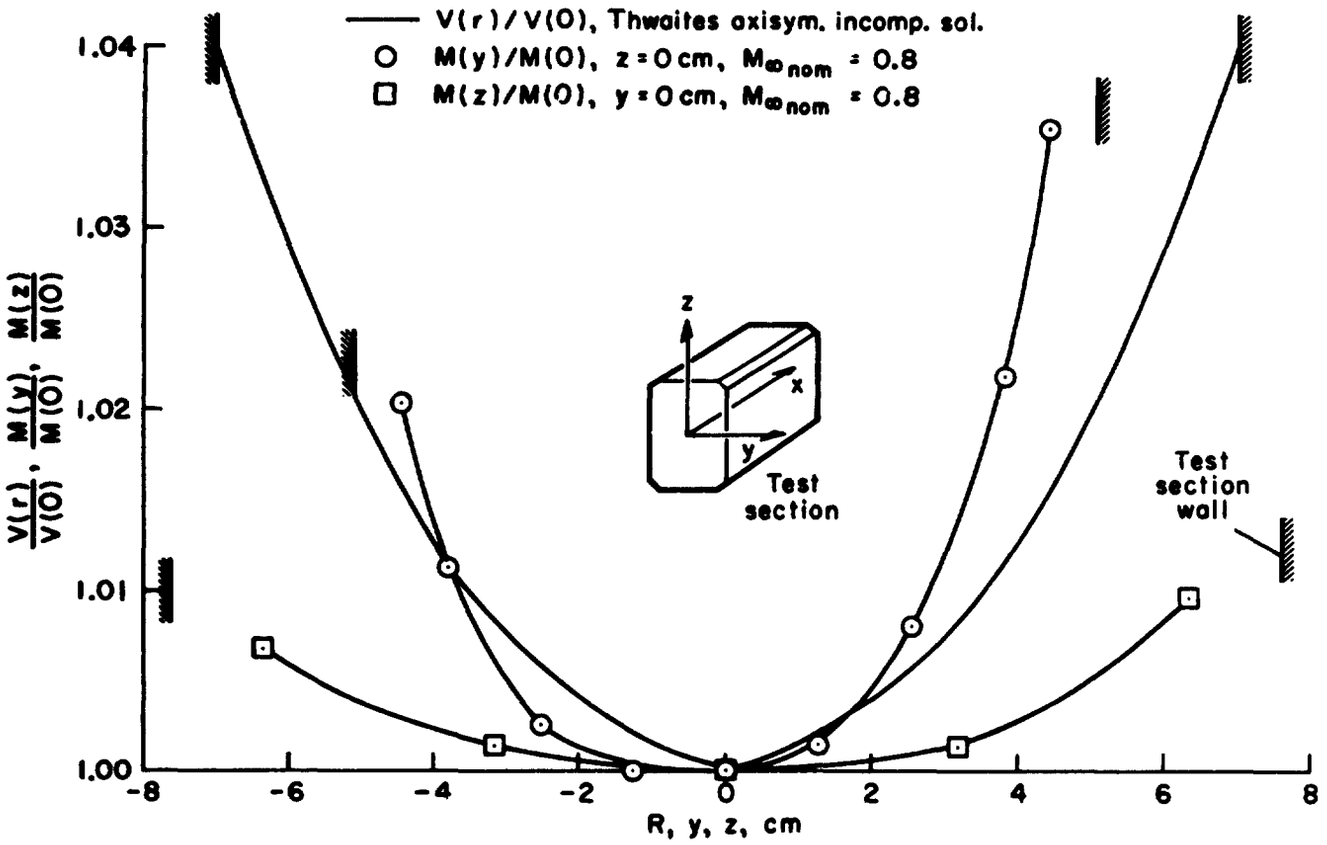

Figure 12. -- Distributions of velocity and Mach number ratio across test-section entrance (x = 0 cm).

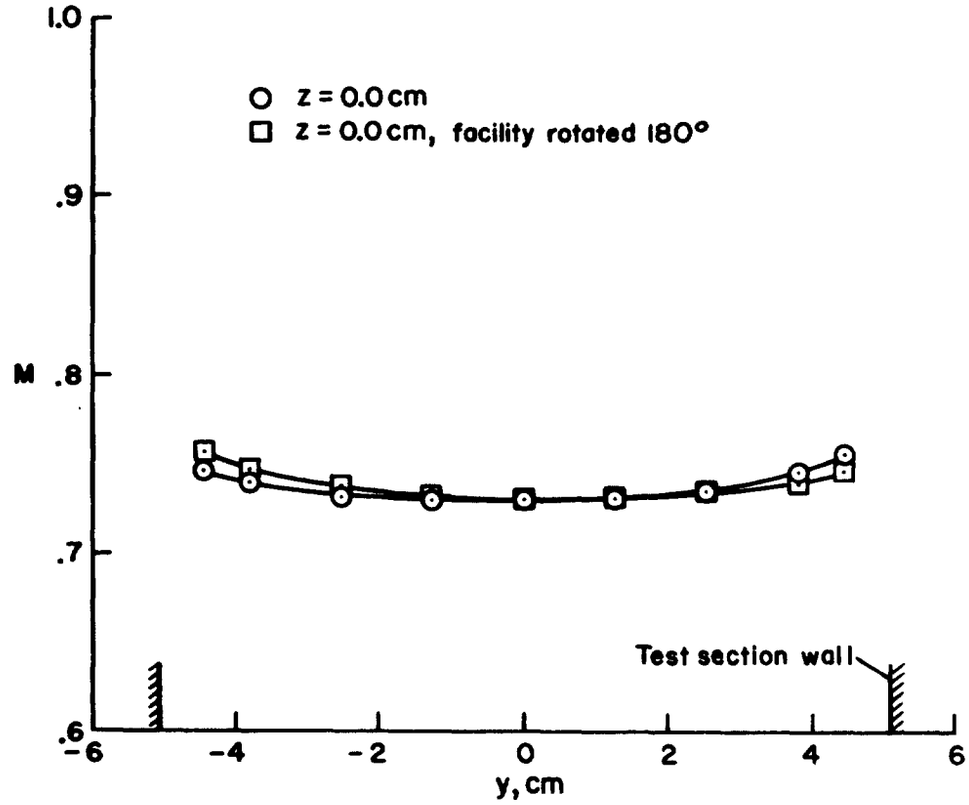

Figure 13. – Effect on Mach number distribution at test-section entrance (x = 0 cm) of rotating facility 180°; $M_{\infty_{nom}} = 0.8$.

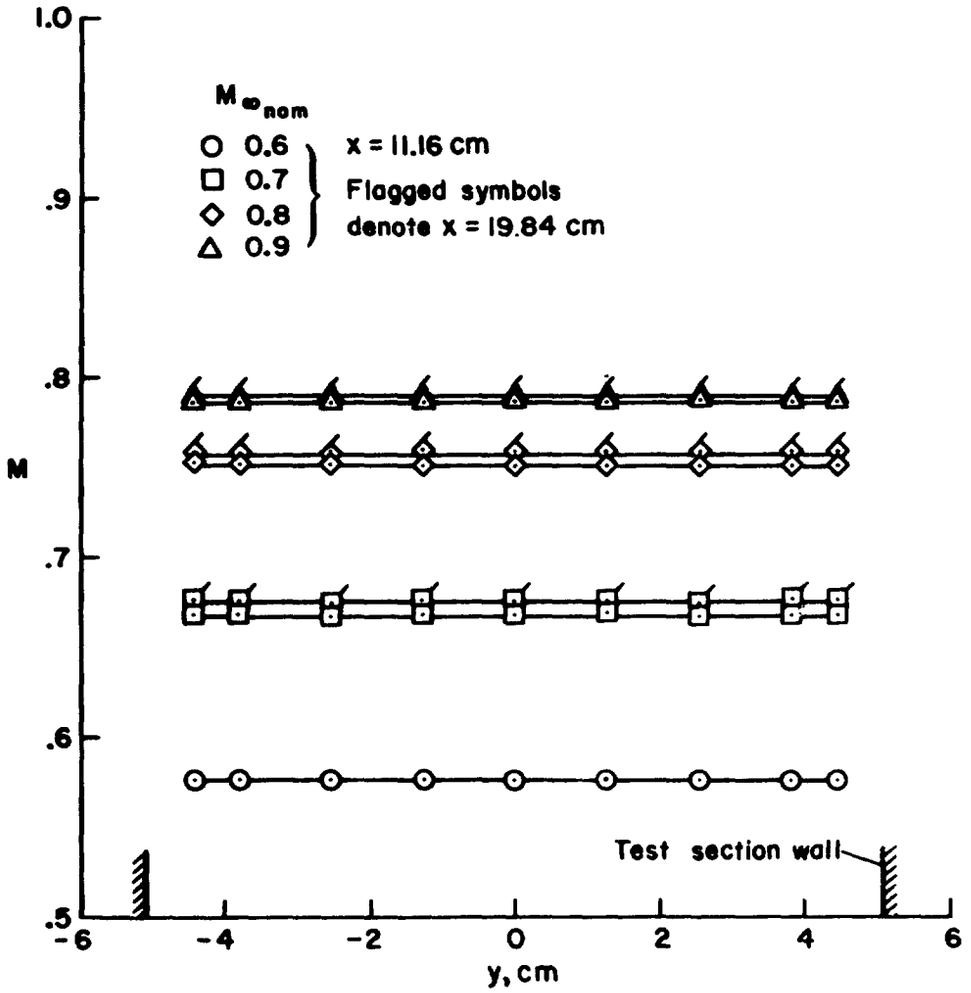

Figure 14. – Horizontal Mach number distributions across center of test-section (z = 0 cm) at two downstream locations.

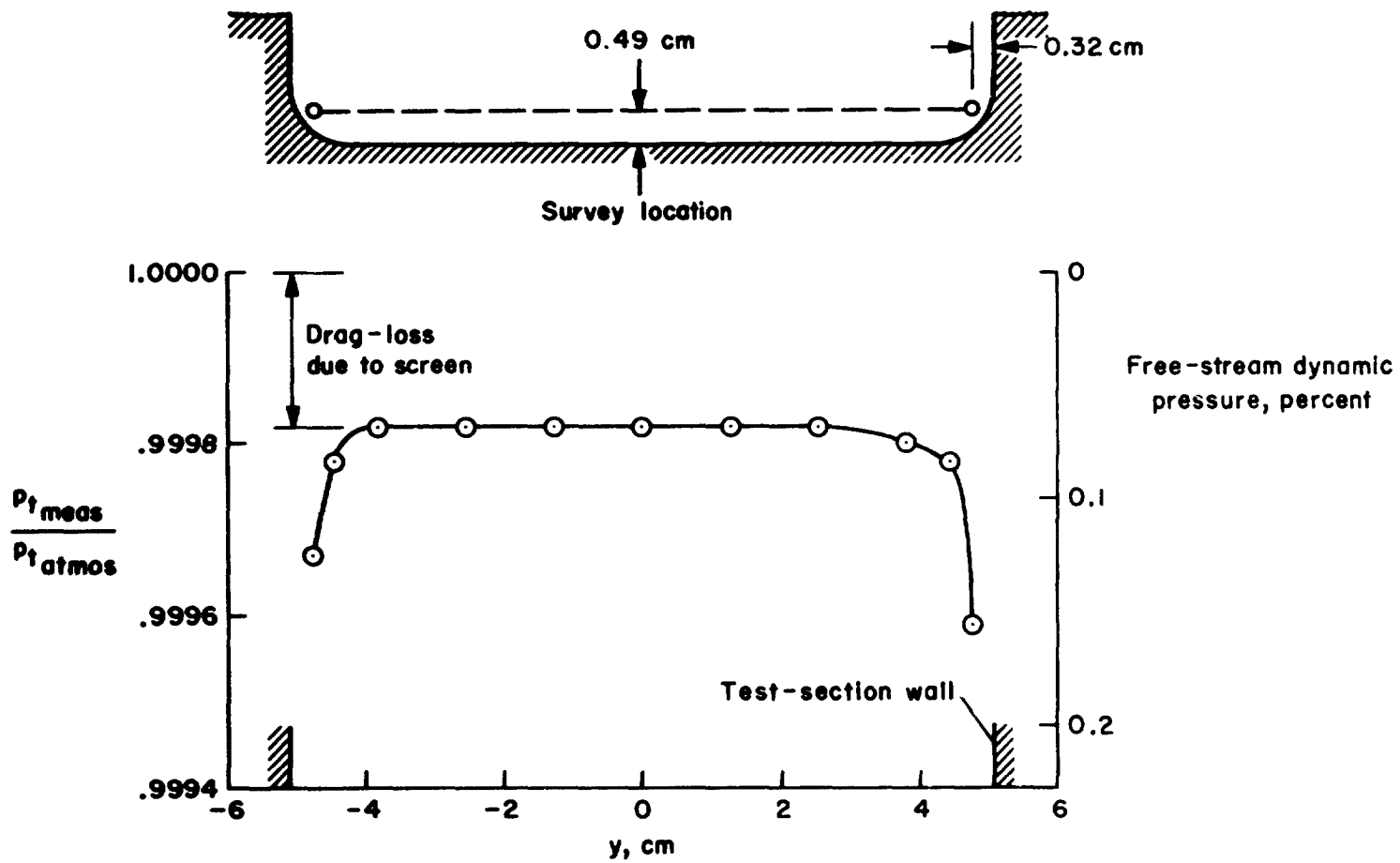

Figure 15. – Total-pressure survey near bottom wall at test-section entrance; $M_{-_{nom}} = 0.8$.

(a) View downstream into test section

Figure 16 Photographs of typical oil-flow patterns on surfaces of pilot facility $M_{nom} = 0.8$

(b) View of test-section wall in region of choke inserts

Figure 16. Concluded